Surface structure and water adsorption on $Fe_3O_4(111)$: Spin-density functional theory and on-site Coulomb interactions

M. E. Grillo,[1] M. W. Finnis,[2] and W. Ranke[3]
[1]*Centro de Quimica IVIC, Apartado 21827, Caracas 1020 A, Venezuela*
[2]*Department of Materials, Imperial College, 46812 Exhibition Road, London SW7 2AZ, United Kingdom*
[3]*Fritz-Haber-Institut der Max-Planck-Gesellschaft, Faradayweg 4-6, D-14195 Berlin, Germany*
(Received 20 December 2007; published 8 February 2008)

The surface structure of magnetite $Fe_3O_4(111)$ in contact with oxygen and water is investigated using spin-density functional theory plus on-site Coulomb interactions. The present results unravel apparent contradictions in the experimental data regarding the equilibrium stoichiometry of the bare surface termination. Both for 298 and 1200 K, the equilibrium structure is terminated by $\frac{1}{4}$ monolayer (ML) of iron (Fe) on top of a full oxygen layer, consistent with an earlier low-energy electron diffraction analysis. Nonetheless, the calculated negative slope of the surface energies vs oxygen partial pressure shows that a $\frac{1}{2}$ ML Fe termination would become stable under oxygen-poor conditions at high temperatures, in agreement to interpretation of scanning tunneling microscopy experiments. Initial water adsorption is dissociative and saturates when all Fe sites are occupied by OH groups, while the H atoms bind to surface oxygen. Further, water bridges the OH and H groups resulting in a unique type of H-bonded molecular water with its oxygen forming a hydronium-ion-like structure OH_3^+-OH. This water structure is different from the water dimeric structures found as yet on oxide and metal surfaces for partially dissociated (H_2O-OH-H) overlayers.

DOI: 10.1103/PhysRevB.77.075407 PACS number(s): 68.43.Fg, 68.35.Md, 71.15.Ap

I. INTRODUCTION

The structure and chemistry of the magnetite $Fe_3O_4(111)$ surface have been investigated in numerous experimental studies. It has recently gained importance in spin electronics[1] and catalytic dehydrogenation reactions in the presence of steam.[2] Water appears to be a unique probe molecule for testing its surface termination and adsorption energetics.[3,4] The theoretical description and prediction of these surfaces, which are the subject of this paper, are challenging for several reasons. First, the equilibrium energies and structures depend on the ambient partial pressures of oxygen (p_{O_2}) and water vapor (p_{H_2O}). Furthermore, the bulk material is antiferromagnetic below 860 K, with magnetic moments on iron tetrahedral sites aligned antiparallel to the octahedral sites.[5] To reproduce these features, we require an electronic theory going a little beyond the most standard *ab initio* approaches of density functional theory (DFT) with the generalized gradient approximation (GGA), or the Hartree-Fock (HF) approximation, in order to treat the correlated *d* electrons on iron.

The bulk structure, shown in Fig. 1, represents a cubic stacking sequence $\cdots$ABC$\cdots$ of close-packed oxygen layers. The iron layers consist of tetrahedrally (Fe_{tet1},Fe_{tet2}) and octahedrally (Fe_{oct1},Fe_{oct2}) coordinated atoms. Depending on preparation conditions, experiments have yielded three proposals for surface termination. After annealing a $Fe_3O_4(111)$ single crystal in oxygen at 950 K and then cooling to room temperature, the surface was believed to be oxygen terminated.[6] Preparation by sputtering and annealing for 20 min at 1073 K resulted in a termination ascribed to $\frac{1}{2}$ monolayer (ML) of tetrahedral and octahedral iron ($Fe_{oct1,tet1}$-O_1).[7] This structure was found to be the lowest-energy structure in a HF study.[8] However, the HF bulk band structure did not reproduce the known antiferromagnetic alignment of magnetic moments within the tetrahedral and octahedral sublattices,[9] as indicated by the calculated excess of majority spin electrons. Finally, analysis of the low-energy electron diffraction (LEED) intensities[10] of epitaxial $Fe_3O_4(111)$ films prepared by cycles of iron deposition and oxidation at 1000 K is consistent with a termination by $\frac{1}{4}$ ML

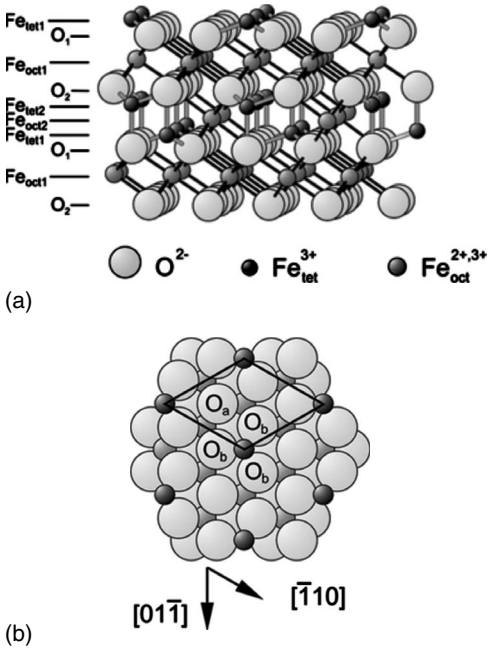

FIG. 1. (a) Side and (b) top views of the $Fe_3O_4(111)$-(1×1) unit cell. The symmetrically inequivalent oxygen atoms O_a and O_b are indicated in the top view. The side view shows the stacking sequence of planes along the [111] direction for the Fe_{tet1} termination. The sequence of planes Fe_{tet1}-O_1-Fe_{oct1}-O_2-Fe_{tet2}-Fe_{oct2}-comprises the surface region.

of Fe atoms (Fe_{tet1}) over a complete oxygen layer O_1.

The interaction of $Fe_3O_4(111)$ with water exhibits very particular characteristics. In a thermal desorption spectroscopy (TDS) study, a first desorption peak shifted with coverage from 282 to 262 K, saturating at $\frac{1}{4}$ ML of H_2O, followed by a second desorption peak shifting from 210 to 190 K and saturating at altogether $\frac{1}{2}$ ML.[3] Based on ultraviolet photoelectron spectroscopy (UPS) data, they were attributed to sequential adsorption of dissociated (γ species) and physisorbed molecular water (β species). Dissociation (γ species) was attributed to the interaction with surface Fe sites. Surprisingly, the γ species are relatively weakly bound and could even be studied in adsorption-desorption equilibrium.[3] Infrared reflection-absorption spectroscopy (IRAS) confirmed their dissociated character. The signature of a hydrogen bond appears only when the β species are coadsorbed, and the formation of a particular kind of water dimer was proposed, combining the γ and the β species.[4]

In the first stage of the theoretical study reported here, we investigate the effect of the experimental parameters, p_{O_2} and T, on the thermodynamic stability of selected $Fe_3O_4(111)$ bare surface terminations. In the second stage, the observed T and p_{H_2O} dependencies of the equilibrium water coverage $\Theta(H_2O)$ of the surface are addressed. The surface stability is accessed by evaluating the Gibbs excess free energies $\sigma(T,p_{O_2},p_{H_2O})$ as a function of the experimental parameters for different magnetite (111) terminations.

II. BULK STRUCTURE

The total energies of periodic blocks of atoms are calculated with DFT and the GGA, with special treatment of on-site Coulomb interactions for d electrons on Fe, using the so-called GGA+U approximation.[11] A value for the $(U-J)$ parameter of 3.8 eV (Ref. 12) was used for all Fe throughout the calculations, which were all done with the all-electron projector-augmented wave method (PAW)[13] as implemented in the VASP package.[14] A kinetic energy cutoff of 400 eV for the plane-wave basis set was adopted. Grids of $(7\times7\times7)$ and $(3\times3\times1)$ special points for Brillouin zone integrations were used for the bulk and surface calculations, respectively. The total energy versus volume of bulk magnetite in the cubic inverse spinel structure $Fd\bar{3}m$ was fitted to the Birch-Murnaghan equation of state. The lattice constant (8.470 Å) and bulk modulus (177.0 GPa) thereby obtained are consistent with the experimental values[15] of 8.3956 Å and 181 GPa, respectively. The electronic band structure shows that magnetite is a semimetallic ferrimagnet caused by the antiferromagnetic exchange interaction between the Fe ions at the tetrahedral (A) and octahedral (B) sites. The net spin density on muffin-tin spheres at the A sites of 4.017 and the total spin density in a primitive cell of 8.000 agree well with the reported magnetic moments[9] of 3.82 and 8.10μ_B, respectively.

III. MAGNETITE $Fe_3O_4(111)$ SURFACE TERMINATIONS

The bare surfaces are modeled by slabs, which are periodic within the surface plane and periodically separated by 15 Å of vacuum along the [111] direction. For each of the calculated $Fe_3O_4(111)$ terminations, a slab therefore includes two equivalent (111) surfaces. For the $\frac{1}{4}$ ML Fe_{tet1} termination, a complete two-dimensionally periodic unit is defined as surface region, comprising one surface Fe_{tet1} layer and the upper half of the slab (shown in Fig. 1). This means that the topmost five interlayer distances within the surface region are optimized throughout the calculations. The similar periodic unit of the lower half slab is defined as the bulk region. The $Fe_{oct2,tet1}$ termination is obtained by adding a further $\frac{1}{4}$ ML octahedrally coordinated iron atoms on both slab surfaces. The close-packed oxygen termination underneath (O_1-Fe_{oct_1}-) is obtained by removing the iron layers on both slab surfaces. For each of the calculated terminations, the atomic coordinates in the planes within the surface region are allowed to relax, while the atoms in the planes within the bulk region are kept fixed at their *ab initio* bulk positions.

The stability of the bare surfaces is analyzed in terms of the dependence of the surface excess Gibbs free energy $\sigma(T,p_{O_2})$ (referred to simply as "the surface energy") on T and the chemical potentials of its components, magnetite or iron ($\mu_{Fe_3O_4},\mu_{Fe}$) and oxygen (μ_O). These chemical potentials are fixed by the chosen value of p_{O_2}. Thus, σ is given by

$$\sigma(T,p_{O_2}) = \frac{1}{A_s}\left(G_s' - \frac{N_{Fe}}{6}\mu_{Fe_3O_4}(T)\right) - \frac{1}{2}\Gamma_O\mu_O(T,p_{O_2}),$$

with $G_s' = G_s - \frac{1}{2}G_s^b$, where G_s stands for the total Gibbs free energy of the material slab; G_s^b denotes the total Gibbs free energy of the slab with *all* ion coordinates fixed at their bulk-truncated positions. G_s' is therefore the Gibbs energy of the surface region defined above. N_{Fe} and N_O are the numbers of iron and oxygen atoms, respectively, in the slab of surface area A_s, and $\mu_{Fe_3O_4}$ stands for the chemical potential of bulk magnetite at standard conditions. Γ_O is the surface oxygen excess with respect to a stoichiometric surface termination, which is defined as[16] $\Gamma_O = \frac{1}{A_s}\left(N_O - \frac{4}{3}N_{Fe}\right)$. The range of oxygen chemical potentials is constrained by the equilibrium of bulk magnetite. Therefore, the minimum $\mu_O(\text{gas})$ is that corresponding to the maximum μ_{Fe}, at which metallic iron would condense at the surface, $\mu_O(\text{gas}) = \frac{1}{4}(\mu_{Fe_3O_4,\text{bulk}} - 3\mu_{Fe,\text{bulk}})$.

The dependence of the oxygen chemical potential on the environmental parameters, p_{O_2} and T, is obtained from the thermodynamic cycle for magnetite formation as implemented previously for α-Al_2O_3.[17] Following the scheme described in detail in Ref. 17, $\mu_O(T,p_{O_2})$ (per atom) is given by

$$\mu_O(T,p_{O_2}) = \frac{1}{4}[\mu^\circ_{Fe_3O_4}(T_1) - \Delta G^\circ_{Fe_3O_4}(T_1) - 3\mu^\circ_{Fe}(T_1)] + \Delta\mu^\circ_O(T) + \frac{1}{2}k_BT\ln(p_{O_2}/p^\circ),$$

where the reference temperature (T_1) is taken here to be the standard value (T°) of 298.15 K, and p° is the standard pressure of 1.013 bar. The change $\Delta\mu^\circ_O(T)$ in the chemical potential of oxygen with T relative to its standard state is given to high accuracy by the expression for an ideal diatomic

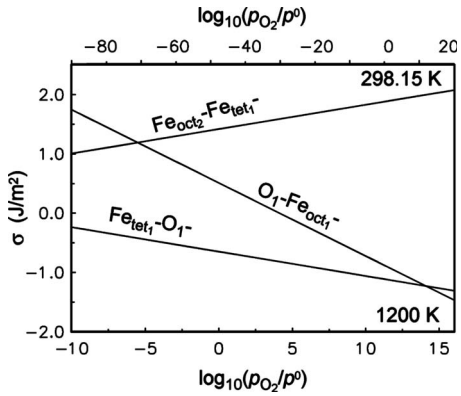

FIG. 2. Surface energies σ vs $\log_{10}(p_{O_2}/p^\circ)$ at 298.15 K (top x axis) and 1200 K (bottom x axis) for the $\frac{1}{4}$ ML (Fe_{tet1}-O_1-) and $\frac{1}{2}$ ML (Fe_{oct2}-Fe_{tet1}-) Fe-terminated and the (O_1-Fe_{oct_1}-) oxygen-terminated surfaces.

gas.[17] The standard Gibbs free energy of formation of bulk magnetite $\Delta G^\circ_{Fe_3O_4}(T_1)$ is obtained from experimental data.[18] The chemical potentials of bulk magnetite $\mu^\circ_{Fe_3O_4}$ and that of bulk iron μ°_{Fe} have been approximated by the calculated internal energies at 0 K.

The calculated surface energies vs p_{O_2} at 298.15 and 1200 K for the three considered terminations are displayed in Fig. 2. The results show that the Fe_{tet1}-terminated surface has the lowest surface energy over the range of relevant oxygen pressures at both temperatures. Nevertheless, at room temperature, the negative slope of energy versus p_{O_2} of the O-terminated surface brings it almost down to the lowest energy (as shown in Fig. 2), and entropic terms ignored in the present theory could tip the balance either way, or an intermediate structure might dominate. At 1200 K, the calculated σ of the $Fe_{oct2,tet1}$ termination below 10^{-6} mbar is lower than that of the close-packed oxygen layer. This is consistent with the disappearance of close-packed oxygen layers coexisting with the Fe_{tet1} termination at oxidation temperatures above 1000 K as observed by scanning tunneling microscopy on epitaxial Fe_3O_4 films.[21] Nonetheless, the rates at which oxygen and iron evaporate from the surface might be decisive in the observed final surface stoichiometry. In that case, the $Fe_{oct2,tet1}$-terminated surface would appear under oxygen-poor conditions at high temperatures if the oxygen evaporation rate is much faster than that of iron.

The iron (Fe_{tet1}) and oxygen (O_1) layers within the surface region relax inward toward the Fe_{oct1} plane underneath. These relaxations bring about large procentual changes in the interlayer spacings such as that calculated for the (0001) surface of hematite (α-Fe_2O_3).[20] However, the absolute changes in the Fe-O bond distances are rather small. Within the directional bonding network of Fe_3O_4, each oxygen ion binds to one tetrahedral (1.898 Å) and three octahedral (2.081 Å) iron cations, respectively. Therefore in Table I, the calculated Fe-O bond lengths are compared to those determined by LEED for the Fe_{tet1} termination. Since oxygens in the O_2 plane within the surface region are involved in bonds with at least one iron in the bulk region (fixed coordinates), variations in the Fe-O bond lengths within this layer cannot be *quantitatively* compared to the LEED values. The calculated Fe-O bond length contraction in the topmost surface layers might be seen as a stabilization mechanism that reduces the electrostatic energy around the surface.[19] Inward relaxation of the topmost surface layers is commonly found in polar surfaces such that calculated for α-Fe_2O_3(0001).[20]

TABLE I. Calculated (GGA+U) and LEED (Ref. 10) Fe–O bond lengths (Å) within the surface region of the slab corresponding to the bulk repeat unit of the Fe_{tet1} termination. Percentages of the corresponding *ab initio* bulk values are given for the theoretical data. The experimental errors in the LEED determined layer distances are reported in Ref. 2.

Interlayer	GGA+U	(%)	LEED
Fe_{tet1}-O_{1a}	1.811	−4.6	1.82
O_{1a}-Fe_{oct1}	1.953	−6.1	1.92
O_{1b}-Fe_{oct1}	1.990	−4.4	1.93
Fe_{oct1}-O_{2b}	2.089	+0.4	2.19
Fe_{oct1}-O_{2a}	2.113	+1.5	2.24
O_{2b}-Fe_{tet2}	1.900	+0.1	1.87
O_2-Fe_{oct2}	2.111	+1.5	2.02

IV. WATER ADSORPTION

A systematic search for energy minima with $\frac{1}{4}$ ML of water adsorbed on the Fe_{tet1}-terminated surface was carried out. Minima were sought both for water adsorbing molecularly and when dissociated into hydroxyls (OH) and protons (H). The lowest-energy structure corresponds to dissociated water with the water OH groups binding to exposed surface Fe via their O atoms at 1.833 Å (see Fig. 3), while the H atoms adsorb on the surface O_a sites at 0.972 Å, as compared to a H-O bond length of 0.975 Å for the hydroxyls on the surface irons. This structure is consistent with interpretations of TDS and UPS data[3] for the dissociated overlayer structure labeled γ water. The adsorption energy (E_{ad}) obtained of 95.40 kJ/mol is consistent with the observed easy dissociation of water on Fe_3O_4(111).[3]

Further, calculated binding configurations for the coadsorption of the dissociation products OH+H and for the initial molecular H_2O adsorption suggest a pathway for water

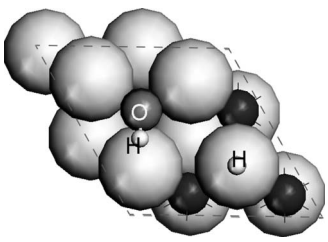

FIG. 3. Top view of the $\frac{1}{4}$ ML dissociated H_2O overlayer on the Fe_{tet1} termination. The dark gray and small white spheres represent the oxygen and hydrogen atoms of the dissociation products (H+OH), respectively. Light gray and black spheres represent the surface oxygen (O) and iron (Fe) atoms, respectively.

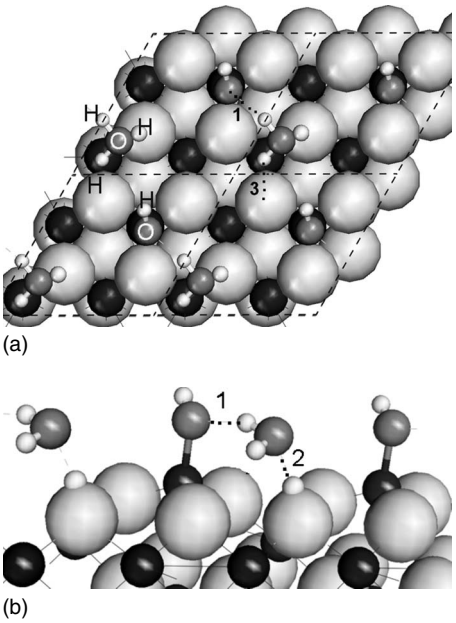

FIG. 4. Side and top views of the $\frac{1}{2}$ ML half-dissociated (H_2O-OH-H) overlayer on the Fe_{tet1} termination. The dark gray and small white spheres represent the oxygen atoms of the partially dissociated overlayer and corresponding hydrogens. Light gray and black spheres represent the surface oxygens (O) and iron (Fe) atoms, respectively. Hydrogen bonds formed by H_2O molecules bridging between the surface hydroxyls (OH) and surface hydrogens (H) are shown. Dashed lines indicate the $Fe_3O_4(111)$-(1×1) surface unit cells.

dissociation within the $Fe_3O_4(111)$-(1×1) unit cell. Initial H_2O molecular adsorption is followed by formation of a transitional dissociated structure with the water protons adsorbed on neighboring O_b sites (see Fig. 1) through diffusion of H atoms. The mobile water protons (H) diffuse eventually over the surface to adsorb on top of the O_a sites. The structures and energetics of the transition configurations will be discussed in detail in a forthcoming article. The proposed water dissociation pathway would be consistent with the slow recombinative second-order desorption kinetics, with the small frequency factor obtained from the γ-water isobar fit to the Langmuir model (Fig. 8 in Ref. 3), and may be the reason for the wide range of β-water adsorption.[3] Hence, the experimental isosteric heats of adsorption $q_{st}(\Theta)$ evaluated from a Clausius-Clapeyron (CC) analysis (60–73 kJ/mol) (see Table I in Ref. 3) may reflect an average value among the populated adsorption sites.

For a $\Theta(H_2O)$ of $\frac{1}{2}$ ML, minima were sought in which $\frac{1}{4}$ ML of molecular H_2O were coadsorbed onto the lowest-energy hydroxylated surface. As opposed to the water dimers expected by interpretation of the H-bond features observed by the IRAS experiments,[4] water monomers are readily anchored onto the hydroxylated surface forming a novel surface "hydronium" (OH_3^+)-like configuration (see Fig. 4). In this structure, molecular water is stabilized by two hydrogen bonds between the surface hydroxyls Fe-OH (1.750 Å, H bond 1 in Fig. 4) and the adsorbed surface hydrogens (1.646 Å, H bond 2), while tilted toward the substrate at 2.672 Å from the closest surface oxygen (H bond 3). The water monomers are constrained to the calculated adsorption position by the H-bond interactions to the substrate, where the O-O distance (2.708 Å) to the next OH group is by about 0.3 Å shorter than that in a gas phase water dimer. The surface hydroxyls are strongly bound to the iron sites with an Fe-O bond (1.875 Å) shorter by about 0.4 Å compared to adsorbed molecular water. At the same time, OH bond lengths in the bridging H_2O monomers of 1.005 and 0.978 Å in length in the adsorbed OH_3^+-OH configuration are long compared to 0.957 Å in gaseous water.

The averaged adsorption energy per H_2O molecule ($E_{ad}^{\gamma+\beta}$) in the OH_3^+-OH overlayer is calculated to be 85.52 kJ/mol, which is very similar to that calculated for half-dissociated overlayers on metals[22] and on $RuO_2(110)$,[23] respectively. The adsorption energy of molecular H_2O over the hydroxylated magnetite surface is calculated to be 75.34 kJ/mol. This indicates a H-bonding contribution of over 80% to the averaged water adsorption energy within the OH_3^+-OH overlayer, as shown already for half-dissociated (H_2O-OH-H) water overlayers on metals.[22]

The experimental isobars for the coadsorption of molecular H_2O (β species) after saturation of the γ species extend over a very wide temperature range. In fact, adsorption isobars for superstructures formed at different relative β coverages could not be distinguished (p. 3231 of Ref. 3). However, LEED measurements showed weak superstructure spots at a relative β coverage corresponding to $\frac{1}{3}$. Hence, the isosteric heat of adsorption values derived from the CC analysis (48–52 kJ/mol) represent average values accounting for all possible transition superstructures for $\Theta(\beta)=\frac{1}{3},\frac{2}{3}$, and 1 as indicated by the dependence of LEED spot intensities on T.

The desorption temperature of β water sequentially adsorbed over dissociated γ water has been accessed in terms of the dependence of its stability on the water partial pressure (p_{H_2O}) and T. The change in surface excess Gibbs free energy $\Delta\sigma_W(T,p_{H_2O})$ with water adsorption becomes

$$\Delta\sigma_W(T,p_{H_2O})=\left(\frac{1}{A_s}\right)\Delta E(T,p_{H_2O}),$$

with

$$\Delta E(T,p_{H_2O})=E_{T,W}-[E_T+N_W\mu_W^o(T,p_{H_2O})],$$

where $E_{T,W}$ and E_T stand for the total energies of the slabs for the water-adsorbed and bare surfaces, respectively, and N_W is the number of adsorbed H_2O molecules. As for the bare surfaces, the total Gibbs free energies of the material slabs have been approximated by the calculated internal energies at 0 K. The equilibrium partial pressure of water determines its chemical potential in the vapor phase $\mu_W(T,p_{H_2O})$, which was estimated using statistical thermodynamics. Hence, the effect of the water adsorption is to reduce the energy of the bare surface by the binding energy per H_2O molecule per unit of surface area with respect to the chemical potential of water in the vapor. The oxygen pressure in the water adsorption experiments is very low. In ultrahigh vacuum instruments, the oxygen partial pressure is given practically by the

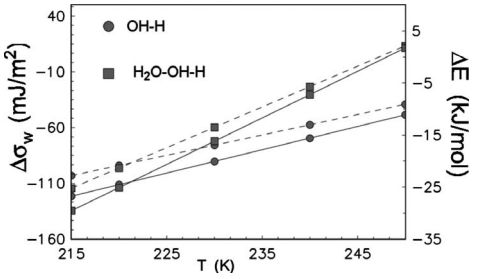

FIG. 5. Surface energy change $\Delta\sigma_W$ with H_2O adsorption and corresponding adsorption energy change ΔE (dashed line) vs T for $\frac{1}{4}$ ML dissociated (OH-H) and for $\frac{1}{2}$ ML half-dissociated (H_2O-OH-H) overlayers on the Fe_{tet1} termination at $p_{H_2O}=10^{-8}$ mbar.

dissociation equilibrium of H_2O, which is strongly endothermic. Hence, the O_2 partial pressure remains very low. The temperature dependence of the dissociation equilibrium of water is shown in Fig. 3(a) of Ref. 24. For instance, at a partial pressure of water of $p_{H_2O}=1\times10^{-6}$ mbar at 300 K, the dissociation O_2 pressure would be just about 1×10^{-25} mbar.

The change in surface excess Gibbs free energy $\Delta\sigma_W(T,p_{H_2O})$ with water adsorption and corresponding energy changes $\Delta E(T,p_{H_2O})$ are plotted as a function of T at the water partial pressure of 10^{-8} mbar in Fig. 5. At temperatures above 220 K (intercept of the energy lines), the energy of the hydroxylated surface is lower than that of the half-dissociated overlayer with respect to the chemical potential of water in the vapor. This temperature of 220 K coincides reasonably well with the observed value of about 200 K at the break of the water adsorption isobars measured at $\Theta(\beta)=\frac{1}{2}$ ML and 1×10^{-8} mbar of H_2O [cf. Fig. 6(a) of Ref. 3].

V. CONCLUSIONS

In summary, density functional theory plus on-site Coulomb interactions (GGA+U) has been used to study the dependence of the equilibrium surface stoichiometry and energetics on the environmental parameters, T, and on the ambient partial pressures of oxygen, p_{O_2}, and water, p_{H_2O}, in order to account for the observed $Fe_3O_4(111)$ surface terminations. The termination exposing $\frac{1}{4}$ ML of Fe atoms over a hexagonal oxygen layer has the lowest Gibbs free energy over the range of relevant oxygen pressures at 298.15 and 1200 K. The observed T dependence of the adsorbed water coverage $\Theta(H_2O)(T)$ is in good agreement with published adsorption isobars taken at $p_{H_2O}=1\times10^{-8}$ mbar. The lowest-energy structures calculated for $\Theta(H_2O)$ of $\frac{1}{4}$ and $\frac{1}{2}$ ML coverages give consistent interpretations of TDS, UPS, and IRAS data. The experimentally determined energetics and kinetics of water adsorption and desorption are well reproduced.

ACKNOWLEDGMENTS

M.E.G. is grateful for financial support by the Fritz-Haber-Institut, Berlin, for the computing resources at the Atomistic Simulation Centre Queen's University Belfast (QUB), where part of this work was carried out, and for prompt technical assistance by Peter Klaver there.

[1] W. Eerenstein, T. T. M. Palstra, S. S. Saxena, and T. Hibma, Phys. Rev. Lett. **88**, 247204 (2002).
[2] W. Weiss and W. Ranke, Prog. Surf. Sci. **70**, 1 (2002).
[3] Y. Joseph, W. Ranke, and W. Weiss, J. Phys. Chem. B **104**, 3224 (2000).
[4] U. Leist, W. Ranke, and K. Al-Shamery, Phys. Chem. Chem. Phys. **5**, 2435 (2003).
[5] V. I. Anisimov, I. S. Elfimov, N. Hamada, and K. Terakura, Phys. Rev. B **54**, 4387 (1996); H.-T. Jeng, G. Y. Guo, and D. J. Huang, Phys. Rev. Lett. **93**, 156403 (2004).
[6] N. Berdunov, S. Murphy, G. Mariotto, and I. V. Shvets, Phys. Rev. B **70**, 085404 (2004).
[7] A. R. Lennie, N. G. Condon, F. M. Leibsle, P. W. Murray, G. Thornton, and D. J. Vaughan, Phys. Rev. B **53**, 10244 (1996).
[8] J. Ahdjoudj, C. Martinsky, C. Minot, M. A. van Hove, and G. Somorjai, Surf. Sci. **443**, 133 (1999).
[9] N. Tsuda, K. Nasu, A. Fujimori, and K. Siratori, in *Electronic Conduction in Oxides*, edited by M. Cardona, P. Fulde, K. von Klitzing, R. Merlin, H.-J. Queisser, and H. Störmer, Solid-State Sciences Vol. 132 (Springer, Berlin, 2000), p. 242.
[10] M. Ritter and W. Weiss, Surf. Sci. **432**, 81 (1999).
[11] S. L. Dudarev, G. A. Botton, S. Y. Savrasov, C. J. Humphreys, and A. P. Sutton, Phys. Rev. B **57**, 1505 (1998).
[12] H. P. Pinto and S. D. Elliott, J. Phys.: Condens. Matter **18**, 10427 (2006).
[13] P. E. Blöchl, Phys. Rev. B **50**, 17953 (1994).
[14] G. Kresse and J. Furthmüller, Comput. Mater. Sci. **6**, 15 (1996); Phys. Rev. B **54**, 11169 (1996).
[15] L. Finger, R. Hazen, and A. Hofmeister, Phys. Chem. Miner. **13**, 215 (1986); H. Okudera, K. Kihara, and T. Matsumoto, Acta Crystallogr., Sect. B: Struct. Sci. **52**, 450 (1996).
[16] M. W. Finnis, Phys. Status Solidi A **166**, 397 (1998).
[17] M. W. Finnis, A. Y. Lozovoi, and A. Alavi, Annu. Rev. Mater. Res. **35**, 167 (2005).
[18] B. S. Hemingway, Am. Mineral. **75**, 781 (1990).
[19] C. Noguera, *Physics and Chemistry at Oxide Surfaces* (Cambridge University Press, Cambridge, 1996).
[20] X.-G. Wang, W. Weiss, Sh. K. Shaikhutdinov, M. Ritter, M. Petersen, F. Wagner, R. Schlögl, and M. Scheffler, Phys. Rev. Lett. **81**, 1038 (1998).
[21] Sh. K. Shaikhutdinov, M. Ritter, X.-G. Wang, H. Over, and W. Weiss, Phys. Rev. B **60**, 11062 (1999).
[22] A. Michaelides, A. Alavi, and D. A. King, Phys. Rev. B **69**, 113404 (2004).
[23] P. J. D. Lindan, N. M. Harrison, and M. J. Gillan, Phys. Rev. Lett. **80**, 762 (1998).
[24] G. Ketteler, W. Weiss, W. Ranke, and R. Schlögl, Phys. Chem. Chem. Phys. **3**, 1114 (2001).